ORNL/TM--8403

DE83 012307

ORNL/TM-8403
Dist. Category UC-20f

Contract No. W-7405-eng-26

FUSION ENERGY DIVISION

ELECTRON HEATING AND SUPERTHERMAL ELECTRON ENHANCEMENT DUE TO ELECTRON-CYCLOTRON HEATING IN ISX-B AT 28 GHz

G. B. Elder
H. Hsuan
Princeton Plasma Physics Laboratory

A. C. England
G. R. Dyer
O. C. Eldridge
J. C. Ezell
E. A. Lazarus
C. M. Loring
C. E. Thomas
J. B. Wilgen
Oak Ridge National Laboratory

A. G. Kulchar
The University of Tennessee

Date Published - May 1983

Prepared by the
OAK RIDGE NATIONAL LABORATORY
Oak Ridge, Tennessee 37830
operated by
UNION CARBIDE CORPORATION
for the
U.S. DEPARTMENT OF ENERGY

CONTENTS

ABSTRACT

A series of electron cyclotron heating (ECH) experiments was performed with a 28-GHz gyrotron on the Impurity Study Experiment (ISX-B) tokamak at Oak Ridge National Laboratory. Up to 70 kW of microwave power was injected into ISX-B from the high field side. Bulk heating was observed with a central temperature rise of ~370 eV from a original temperature of ~600 eV, as measured by Thomson scattering. With ECH and under low density conditions, large nonthermal signals were observed on electron cyclotron emission diagnostics at the first, second, and third harmonics. These signals sometimes became quite large after the end of the ECH pulse. The effects observed can be attributed to relatively small changes in the electron distribution function. The temporal behavior of the enhanced emission is tentatively attributed to the pitch angle scattering of superthermal electrons.

1. INTRODUCTION

During 1980 and 1981 a series of electron cyclotron heating (ECH) experiments was performed with a 28-GHz Varian gyrotron on the ISX-B tokamak. These experiments were an extension of earlier bulk heating[1] and preionization[2] experiments conducted with a frequency of 35 GHz at a similar power level. We report the effects observed and offer some preliminary explanations.

The gyrotron, waveguide system, antenna, and associated equipment are described in Sect. 2, as are the tokamak and its operation. In Sect. 3 the diagnostics are described, with particular attention to the electron cyclotron emission (ECE) diagnostics, from which a major portion of the analysis proceeds. Measurements were made with fundamental, second, and third harmonic detectors. Section 4.1 describes the bulk heating results; Sect. 4.2 describes the experiments in which changes in the electron distribution function were observed by the ECE diagnostics and then gives some possible explanations for these changes. Section 5 contains a summary and conclusions.

2. DESCRIPTION OF THE EXPERIMENTAL EQUIPMENT

2.1 THE MICROWAVE POWER SOURCE

The microwave power source for these experiments was a gyrotron with a frequency of 28 GHz. The tube was a triple-miter-bend VGA-8000 gyrotron with a rated power output of 170 kW (pulsed). However, at the time of its use the power output was about 100 kW at the gyrotron output window. The power supply allowed a pulse length of 100 ms from a capacitor bank energy storage system. The output was into an oversize waveguide with a 6.35-cm (2.5-in.) inside diameter that guided the power to the tokamak. The total waveguide length was about 15.24 m (50 ft). There was one miter bend in the waveguide to change the direction by 90° over the tokamak. The microwave power passed through a water-cooled microwave window into the tokamak vacuum chamber, where it was guided by an additional length of waveguide to a reflecting mirror on the high field side at the midplane. The mirror was oriented to reflect the power into the plasma at an angle of approximately 60° to the field lines. Calorimetric measurements made with a water load at the end of the waveguide showed that only 70 kW of power was delivered to the vacuum window at the tokamak out of 100 kW available at the gyrotron.

A Wengenroth[3] polarizer was used on the mirror to polarize the radiation into the extraordinary mode so that the power would be efficiently absorbed by the plasma in one pass. This polarizer was designed for circular electric waveguide modes such as TE_{01} and TE_{02}, and the VGA-8000 gyrotron was originally designed to generate power in these modes. However, due to the triple-miter-bend construction very little of the power was produced in these modes; hence, the Wengenroth polarizer was probably ineffective in this experiment. In the calculations made for the radiated power, it was assumed that approximately 50% of the power was radiated in the ordinary mode and 50% in the extraordinary mode. A more complete description of the microwave equipment and power supply was given by Campen et al.[4]

2.2 TOKAMAK OPERATION

The tokamak (described in Refs. 1 and 2) was operated under a variety of conditions. However, for a majority of the experiments described here, the magnetic field was adjusted for resonance on the axis, that is, 10.0 kG. The plasma density was adjusted by gas feed to a level below the ordinary mode cutoff density, which is $\sim 1.0 \times 10^{13}$ cm^{-3}. The line-averaged density as measured by a 2-mm interferometer was generally below 6.0×10^{12} cm^{-3}, in order to keep the central density below cutoff. The best results were obtained with this density or lower values. The plasma current was kept low enough to avoid masking any auxiliary heating by high ohmic heating,

ABSTRACT

A series of electron cyclotron heating (ECH) experiments was performed with a 28-GHz gyrotron on the Impurity Study Experiment (ISX-B) tokamak at Oak Ridge National Laboratory. Up to 70 kW of microwave power was injected into ISX-B from the high field side. Bulk heating was observed with a central temperature rise of ~370 eV from a original temperature of ~600 eV, as measured by Thomson scattering. With ECH and under low density conditions, large nonthermal signals were observed on electron cyclotron emission diagnostics at the first, second, and third harmonics. These signals sometimes became quite large after the end of the ECH pulse. The effects observed can be attributed to relatively small changes in the electron distribution function. The temporal behavior of the enhanced emission is tentatively attributed to the pitch angle scattering of superthermal electrons.

1. INTRODUCTION

During 1980 and 1981 a series of electron cyclotron heating (ECH) experiments was performed with a 28-GHz Varian gyrotron on the ISX-B tokamak. These experiments were an extension of earlier bulk heating[1] and preionization[2] experiments conducted with a frequency of 35 GHz at a similar power level. We report the effects observed and offer some preliminary explanations.

The gyrotron, waveguide system, antenna, and associated equipment are described in Sect. 2, as are the tokamak and its operation. In Sect. 3 the diagnostics are described, with particular attention to the electron cyclotron emission (ECE) diagnostics, from which a major portion of the analysis proceeds. Measurements were made with fundamental, second, and third harmonic detectors. Section 4.1 describes the bulk heating results; Sect. 4.2 describes the experiments in which changes in the electron distribution function were observed by the ECE diagnostics and then gives some possible explanations for these changes. Section 5 contains a summary and conclusions.

2. DESCRIPTION OF THE EXPERIMENTAL EQUIPMENT

2.1 THE MICROWAVE POWER SOURCE

The microwave power source for these experiments was a gyrotron with a frequency of 28 GHz. The tube was a triple-miter-bend VGA-8000 gyrotron with a rated power output of 170 kW (pulsed). However, at the time of its use the power output was about 100 kW at the gyrotron output window. The power supply allowed a pulse length of 100 ms from a capacitor bank energy storage system. The output was into an oversize waveguide with a 6.35-cm (2.5-in.) inside diameter that guided the power to the tokamak. The total waveguide length was about 15.24 m (50 ft). There was one miter bend in the waveguide to change the direction by 90° over the tokamak. The microwave power passed through a water-cooled microwave window into the tokamak vacuum chamber, where it was guided by an additional length of waveguide to a reflecting mirror on the high field side at the midplane. The mirror was oriented to reflect the power into the plasma at an angle of approximately 60° to the field lines. Calorimetric measurements made with a water load at the end of the waveguide showed that only 70 kW of power was delivered to the vacuum window at the tokamak out of 100 kW available at the gyrotron.

A Wengenroth[3] polarizer was used on the mirror to polarize the radiation into the extraordinary mode so that the power would be efficiently absorbed by the plasma in one pass. This polarizer was designed for circular electric waveguide modes such as TE_{01} and TE_{02}, and the VGA-8000 gyrotron was originally designed to generate power in these modes. However, due to the triple-miter-bend construction very little of the power was produced in these modes; hence, the Wengenroth polarizer was probably ineffective in this experiment. In the calculations made for the radiated power, it was assumed that approximately 50% of the power was radiated in the ordinary mode and 50% in the extraordinary mode. A more complete description of the microwave equipment and power supply was given by Campen et al.[4]

2.2 TOKAMAK OPERATION

The tokamak (described in Refs. 1 and 2) was operated under a variety of conditions. However, for a majority of the experiments described here, the magnetic field was adjusted for resonance on the axis, that is, 10.0 kG. The plasma density was adjusted by gas feed to a level below the ordinary mode cutoff density, which is $\sim 1.0 \times 10^{13}$ cm^{-3}. The line-averaged density as measured by a 2-mm interferometer was generally below 6.0×10^{12} cm^{-3}, in order to keep the central density below cutoff. The best results were obtained with this density or lower values. The plasma current was kept low enough to avoid masking any auxiliary heating by high ohmic heating,

yet high enough that the electron temperature was adequate for good single-pass absorption. An initial electron temperature of 600 eV was sufficient at these densities, and this was maintained by plasma currents of 60-140 kA.

3. DIAGNOSTICS

Diagnostics used in this experiment include a Thomson scattering system for electron density and temperature measurements, MHD loops, an array of soft x-ray pin diode detectors, and a radiometer array. The ECE diagnostics specific to this experiment are described in Sects. 3.1 and 3.2.

3.1 FUNDAMENTAL AND SECOND HARMONIC CYCLOTRON RADIATION DIAGNOSTICS

One of the primary diagnostics of the electron temperature during 28-GHz heating experiments was ECE. Initial measurements used a 58-GHz millimeter-wave receiver to detect emissions at the second harmonic ($2\omega_{ce}$) of the electron cyclotron frequency. In an effort to obtain a measurement that was less sensitive to nonthermal electron populations, a second detector was added to cover the frequency range of 29-40 GHz, which coincides with the fundamental of the electron cyclotron frequency.

The 58-GHz detector, which had previously been used for 35-GHz ECH experiments,[1] was modified to improve its characteristics. A block diagram of the receiver is shown in Fig. 1. The modified system includes a balanced mixer-preamplifier with an isolated input. In addition, a cut-off waveguide high pass filter was added to reduce interference at 56 GHz, the second harmonic of the heating frequency. Such a second harmonic signal might originate either in the gyrotron itself or from nonlinear plasma processes. This filter provides more than 70-dB isolation at 56 GHz with minimal insertion loss above 58 GHz.

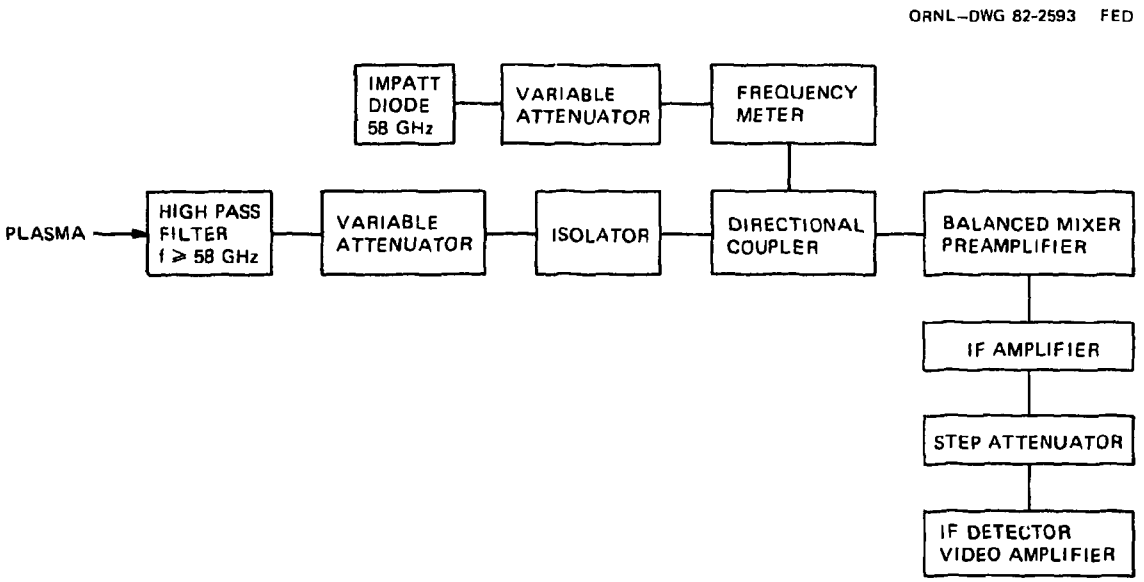

Fig. 1. Block diagram of the second harmonic ECE detection system.

Cyclotron radiation from the plasma was collected and guided to the receiver with an oversized X-band waveguide system, which is described in detail in Ref. 5. The plasma was viewed from the high field side in a direction perpendicular to the toroidal field, and the waveguide was oriented to detect the X-mode polarization ($E \perp B$).

Although second harmonic emission was generally a very useful electron temperature diagnostic for 35-GHz heating experiments, similar measurements for 28-GHz heating are compromised by significantly increased levels of nonthermal radiation. There are two principal reasons for this difference. First, 28-GHz heating requires that the plasma density be lower by 35%, due to wave propagation (cutoff) considerations. Such lower density tokamak operation results in increased populations of nonthermal electrons. Second, the decreased electron density leads to a reduction in the optical depth of the resonant layer, resulting in an increased susceptibility to nonthermal radiation. Fidone[6] has investigated the contribution of nonthermal electron populations to the cyclotron radiation and concludes that the nonthermal radiation can be largely avoided by simply viewing the plasma from the low field side. Even so, if the plasma becomes sufficiently transparent (optically thin), then this geometrical advantage is diminished and the nonthermal radiation becomes evident from all viewing angles.

In summary, by comparison with 35-GHz ECH, the decreased electron densities inherent to 28-GHz heating result in substantially increased levels of nonthermal radiation, and the increased transparency of the resonance layer provides less reabsorption of the nonthermal contributions. For these reasons, the second harmonic detector that was very valuable for 35-GHz ECH turned out to be of marginal value for 28-GHz heating.

One approach to improving the utility of cyclotron emission diagnostics is to observe emission at the fundamental electron cyclotron frequency in addition to the second harmonic. At $2\omega_{ce}$, the radiation rate of individual electrons is proportional to their energy, so that a relatively small number of energetic electrons from the tail of a nonthermal energy distribution can dominate the radiation. In contrast, with the proper viewing angle with respect to the toroidal field, the radiation rate of electrons at the fundamental electron cyclotron frequency is independent of their energy, resulting in a more favorable weighting toward the bulk of the energy distribution.

To explore the possibility of using ECE at the fundamental electron cyclotron frequency as an electron temperature diagnostic, a superheterodyne microwave receiver covering the frequency range of 26.5-40 GHz was constructed. A block diagram of this system is shown in Fig. 2. The local oscillator was a backward wave oscillator (BWO) tube, which was electronically tunable over a frequency range of 26.5-40 GHz. The intermediate frequency (IF) was 160 MHz with an IF bandwidth of 100 MHz, so the double sideband receiver was sensitive to radiation in two 100-MHz bands located 160 MHz to either side of (above and below) the local oscillator frequency. To avoid possible interference from the high levels of 28-GHz heating power, a cutoff waveguide high pass filter was constructed to provide at least 70-dB isolation at 28 GHz with minimum insertion loss above 29 GHz. In addition, a low pass harmonic filter with a stop band of 47-120 GHz was added to preclude the detection of nonthermal radiation at higher harmonics of the electron cyclotron frequency. Radiation from the plasma was collected by a horn viewing from the high field side at an angle of 60° with respect to the toroidal field. The horn was oriented to receive the X-mode polarization, and the radiation was guided to the receiver using a standard size (WR-28) waveguide.

3.2 THE THIRD HARMONIC DIAGNOSTIC

In determining the design requirements of the superheterodyne receiver used to observe the third harmonic emissions on ISX-B, it was necessary to estimate the ECE intensity in the third harmonic. The third harmonic emissions were measured with a detector bank.

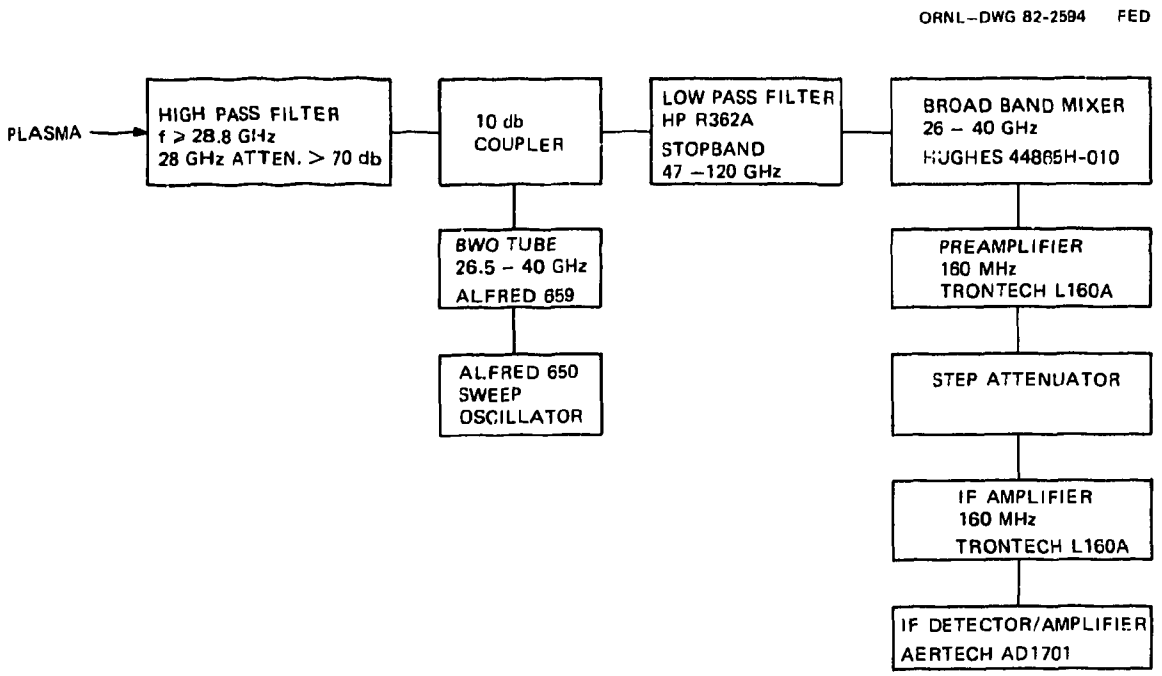

Fig. 2. Block diagram of the fundamental ECE detection system.

The detector bank was designed with five channels, each consisting of a narrow band-pass filter, an E&H tuner, and a Schottky barrier diode detector. The filters were single-pole devices designed and built at Princeton Plasma Physics Laboratory (PPPL). When the corresponding E&H tuner and detector were properly adjusted, the resulting band of frequencies was very narrow. A typical filter had a 3-dB half-bandwidth of ~100 MHz with a center frequency of 88.9 GHz, while the damping at $\Delta f > 200$ MHz was over −30 dB. The final sensitivity to a signal at the entrance to the system was greater than −100 dBm/MHz.

This system shared the waveguide and antenna structure of the second harmonic detector and was connected via a 3-dB directional coupler. Toroidal and poloidal views of the antenna system installed on ISX-B are shown in Figs. 3 and 4, respectively. The results of these measurements[7] clearly showed that for a normal ohmically heated plasma the emission level was below the sensitivity of the system. However, it was noted that in shots with large numbers of runaway electrons there was a signal at the very minimum level required for detection. As a result, the necessary sensitivity of the superheterodyne receiver was estimated to be greater than −110 dBm/MHz.

The heterodyne system, shown in Fig. 4, was designed to provide information about the third harmonic emission, concentrating on the region close to the third harmonic of the 28-GHz heating frequency. A Tektronics 7L12 spectrum analyzer (SA) with a frequency range of 0.1-1.8 GHz was used for the IF detector. The rest of the components in the receiver also needed to have this IF range. Although this is not a standard IF bandwidth, a Hughes single-ended mixer with the requisite characteristics was available. A Gunn diode, chosen for its stability and simple implementation requirements, was used for the local oscillator.

A wide band IF amplifier was chosen to amplify the signal from the mixer before it reached the SA. Furthermore, the SA was located immediately adjacent to the mixer in order to minimize cable losses at the higher frequencies. A high pass filter was used to separate the upper and lower sidebands, with approximately 10-dB attenuation over the lower sideband. The final sensitivity of this system allowed the detection of a −120-dBm signal over the frequency range of 83.5-85.1 GHz, with a 3-MHz IF bandwidth as determined by the SA. This system is shown in Fig. 4.

ORNL–DWG 82-2597 FED

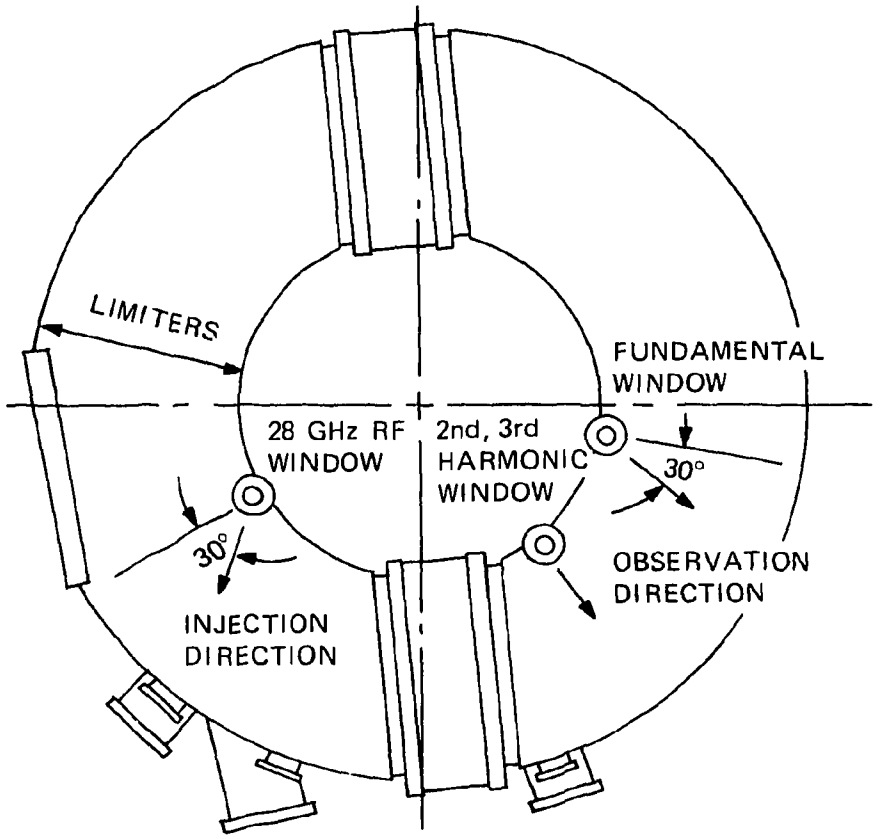

Fig. 3. A top view of the tokamak showing the location of the detection systems and where the ECH is introduced.

The system was attached to ISX-B in the same manner as the detector bank. On the final day of operation, a semiflexible, low loss cable was run from the machine platform to the diagnostic racks to allow the SA to be moved to a position where its operational mode could be adjusted more readily. The signals from the existing SA and from another one that became available were fed to the ORNL computer system for a permanent record. This was accomplished through a fast digitizer, allowing a frequency resolution in the upper sideband of approximately 3 MHz.

4. ANALYSIS AND RESULTS

4.1 BULK HEATING EXPERIMENTS

In this series of experiments it proved very difficult to measure the electron temperature by Thomson scattering due to the low power and low density. The operating window was found to be very narrow. The magnetic field was set for a cyclotron resonance very close to the axis (10.2 kG). The plasma current had to be kept low enough to avoid masking the ECH effect, yet high enough to provide an electron temperature T_e adequate for good single pass absorption. An initial T_e of 600 eV was sufficient, and the measured temperature rise was 370 ± 110 eV. The plasma density had to be kept low ($\simeq 6 \times 10^{12}$ cm^{-3}) to avoid cutoff (i.e., to provide accessibility) for the

ORNL-DWG 82-2596 FED

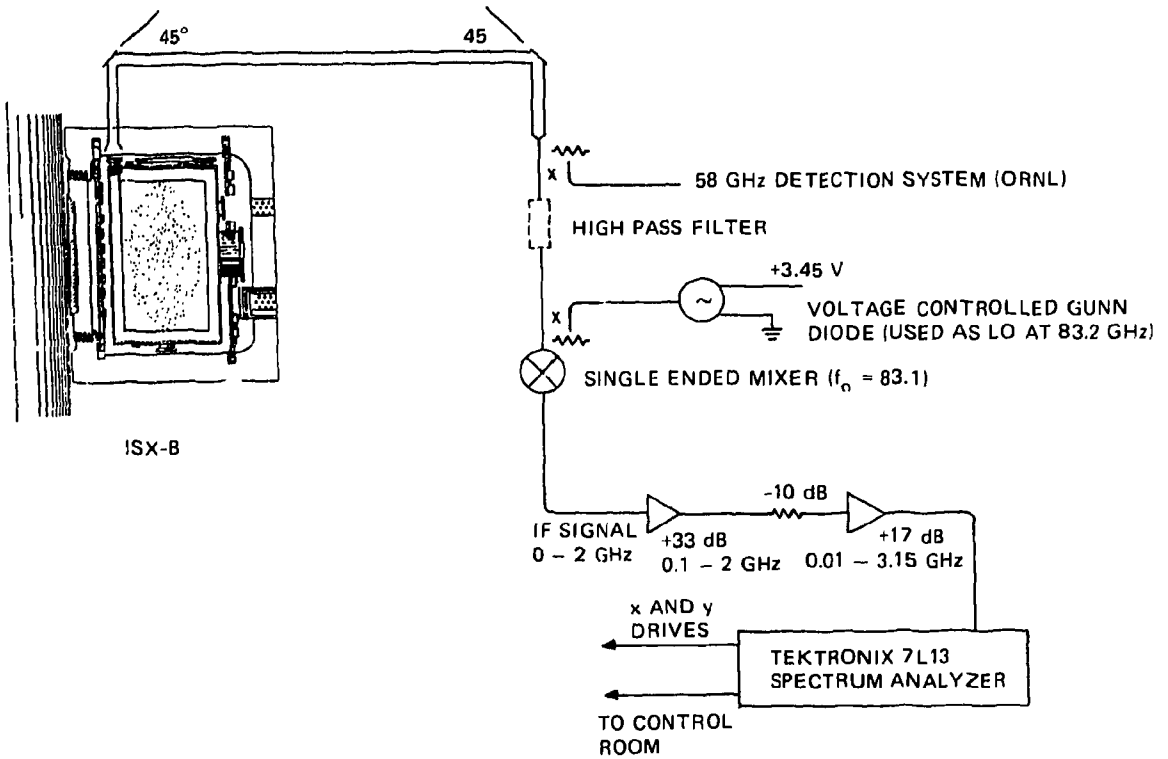

Fig. 4. The third harmonic system on ISX-B.

ordinary mode to keep the total number of particles small. Due to this low density, only a central temperature $T_e(0)$ could be measured by Thomson scattering.

During the experiment the loop voltage was observed to drop ≈30% (see Fig. 5), in rough agreement with the temperature rise. The density also dropped, as it did on ISX-B in previous experiments at 35 GHz,[1] on the JFT-2 experiment at 28 GHz,[8] and on T-10 at 85 GHz.[9] Figure 6 shows the density drop with ECH (dotted line) compared with the normal density with no ECH (solid line). There is still no satisfactory understanding of this density drop, which was observed on both the laser measurement and the 2-mm interferometer.

Without a full profile, only a rough energy balance could be made. If it is assumed that 70 kW entered the plasma, then between 35% and 70% of this power was deposited in the plasma.

No heating effect was observed for off-axis ($B \neq 10.2$ kG) heating, and there was no evidence of profile broadening or instability suppression. However, due to the low power, these effects would not be easily observed.

4.2 ECE MEASUREMENTS

This section is divided as follows: first, the general form of the detected signals is given for all three harmonics. Second, the most salient points to be noted in the entire collection of data are briefly described. We discuss only the major features of these signals and leave more detailed and complete discussions for a later publication.

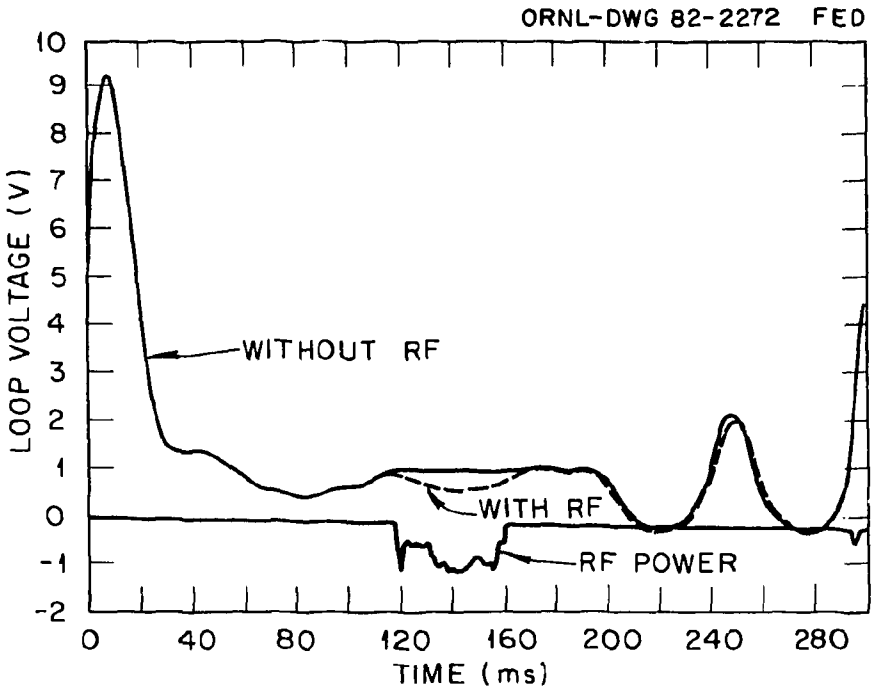

Fig. 5. Loop voltage vs time for a case with no ECH (solid line) and for the case in which ECH produced a measurable temperature rise (dotted line). With ECH, the loop voltage drops about 30%. The curves have been smoothed with a Gaussian filter tc remove electrical noise due to the feedback.

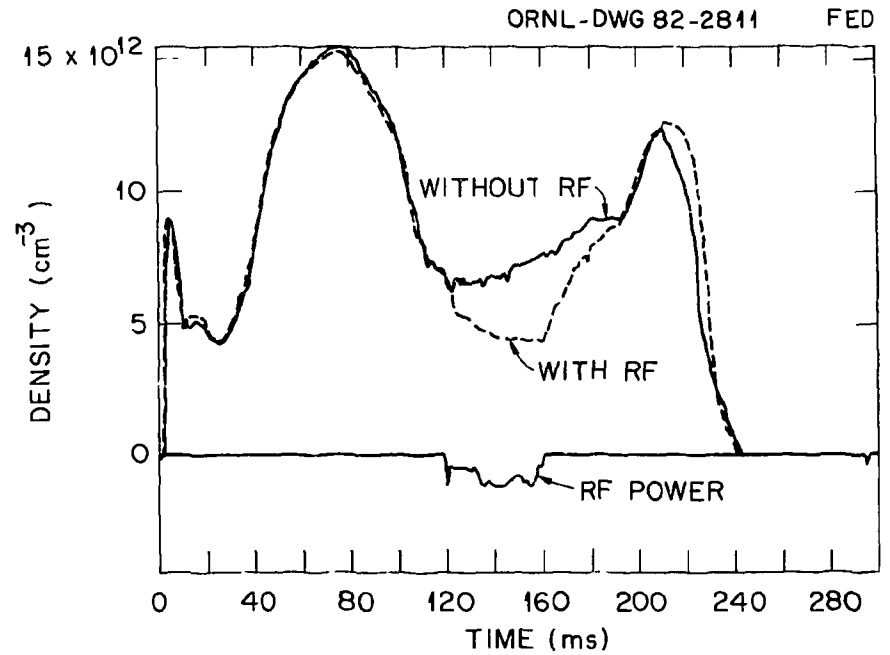

Fig. 6. Electron density vs time for a case with no ECH (solid line) and for the case in which ECH produced a measurable temperature rise (dotted line).

4.2.1 Experimental Results

Figures 7-9 show the fundamental, second harmonic, and third harmonic signals for representative shots. The line-averaged density for typical operating parameters is shown in Fig. 10. The dotted line indicates the signal for the case of no ECH, and the solid line shows the signal when ECH is applied. The ECH pulse was applied at 130 ms and lasted 40 ms, except for the case in Fig. 8, for which it was on for 10 ms. Although the three cases have quite major differences, we first consider the similarities.

In both the fundamental and the second harmonic traces, the signal rises at the beginning of the discharge and then settles down to a fairly constant value (see Figs. 7-9). When there is no ECH, the second harmonic signal tracks the temperature of the plasma (as determined by Thomson scattering and soft x-ray monitors) quite closely, and it is reasonable to assume that it represents the classical blackbody radiation expected in this frequency range. The fundamental signal increases by about twice as much as the second harmonic signal (see Fig. 8) and is probably being affected by a tail on the electron distribution. Such effects have been predicted by Fidone et al.[10] and observed on the Tokamak Fontenay-aux-Roses (TFR)[6] and the Princeton Large Torus (PLT).[11] The fundamental and second harmonic signals decrease at the end of the discharge when the density increases (see Fig. 7), a result of the plasma cutoff for the extraordinary mode and a general cooling of the plasma. The density increase at the end was for suppression of runaways.

However, when there is ECH, this behavior is often modified. A large signal rises after the ECH pulse (see Fig. 9) and then decreases before the density increase would be expected to cut off the signal. This signal does not appear on the soft x-ray spectrum or the Thomson scattering temperature, and it appears to be a large increase in the perpendicular energy of the few electrons in the tail of the distribution.

A large noisy signal during ECH is seen in all three figures and in all the harmonics, although it is much weaker in the third harmonic signal. Studies of the 28-GHz gyrotron characteristics have shown that modes at 29, 30, and 31 GHz can develop during operation. Since these modes would result in a strong signal in the passband of the fundamental system, it is unlikely that any other information can be extracted from the signal for this period. Similarly, the second harmonic signal may be affected by the second harmonic of these gyrotron modes.

On the other hand, the third harmonic signal is close enough to the third harmonic of the primary gyrotron frequency that higher harmonics of these modes should not affect it. Still, some large amplitude signals are seen during the period that the gyrotron is on, and it is probable that these signals are due, at least in part, to noise from the gyrotron. Considering the sensitivity of the receiver, a gyrotron-produced sideband that was -110 dB from the peak would still saturate the system. The spectrum of the third harmonic was taken with the SA; a typical trace, averaged over a number of shots and with background noise and the no-ECH signal removed, is shown in Fig. 11. The sawtooth waveform at the bottom of the picture is the SA drive, and the upper traces are series of frequency sweeps from 83.8 to 85.1 GHz with the frequency ramped by the SA drive. The details of the spectrum during the gyrotron pulse are still being studied, with the hope that peaks due to gyrotron noise can be eliminated. Special attention is being paid to the possibility of detecting daughter waves of a parametric decay similar to those observed at Massachusetts Institute of Technology (MIT) on Versator.[12]

The third harmonic signal is also different in that frequently there is no signal until the ECH begins (see, for example, Figs. 7 and 8). The condition for the appearance of a pre-ECH signal is a very low density during the early part of the discharge. The second harmonic signals are the same in both cases (i.e., the temperature is the same), and the density change is not enough to account for the difference in the third harmonic signal. The optically thin third harmonic radiation scales as[13]

$$I_{ex}^{(3)} \propto n_e T_e^3 , \qquad (1)$$

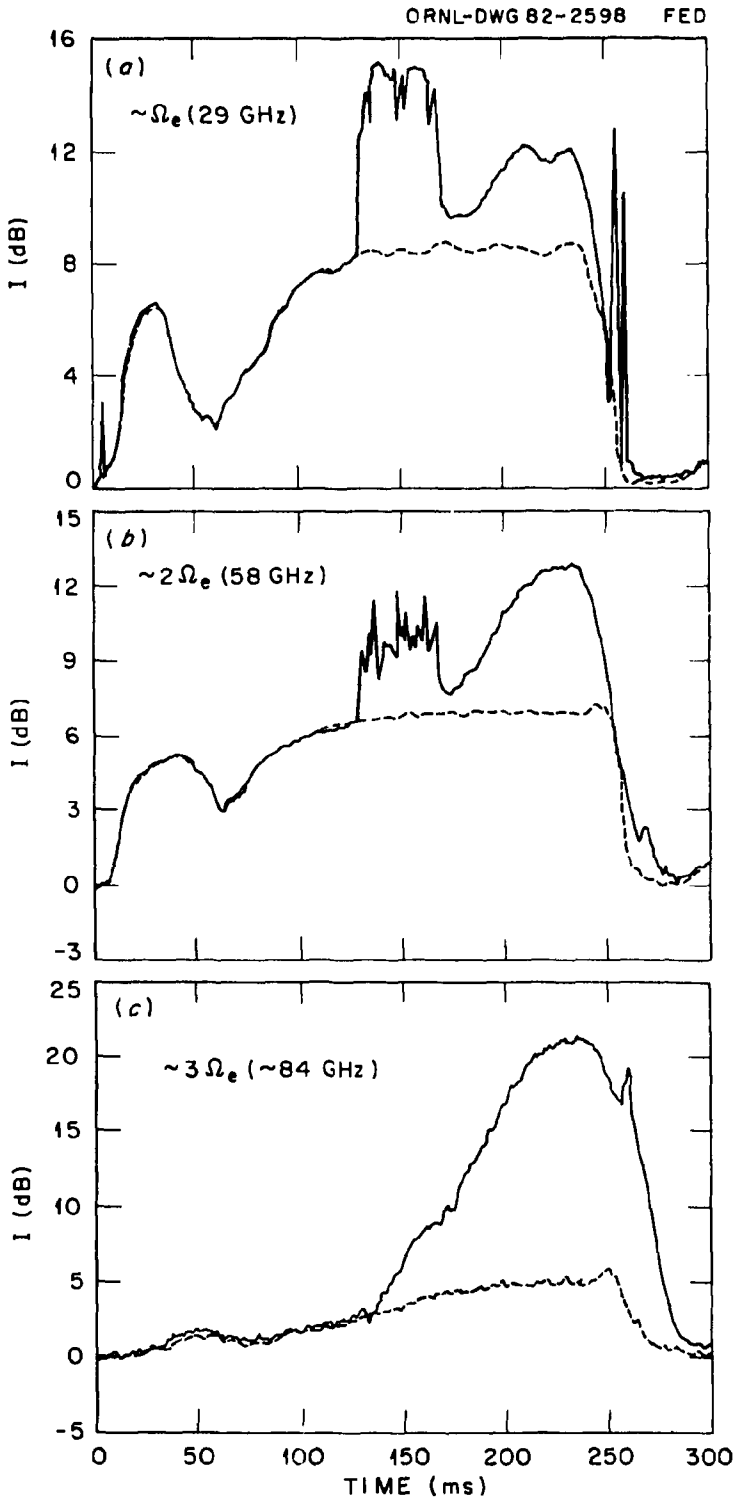

Fig. 7. ECE during a typical discharge ($n_e \sim 5.6 \times 10^{12}$ cm^{-3}) for cases with no ECH (solid line) and with an ECH pulse lasting 40 ms (dotted line). *(a)* Fundamental signal. *(b)* Second harmonic. *(c)* Third harmonic at 84.5 GHz.

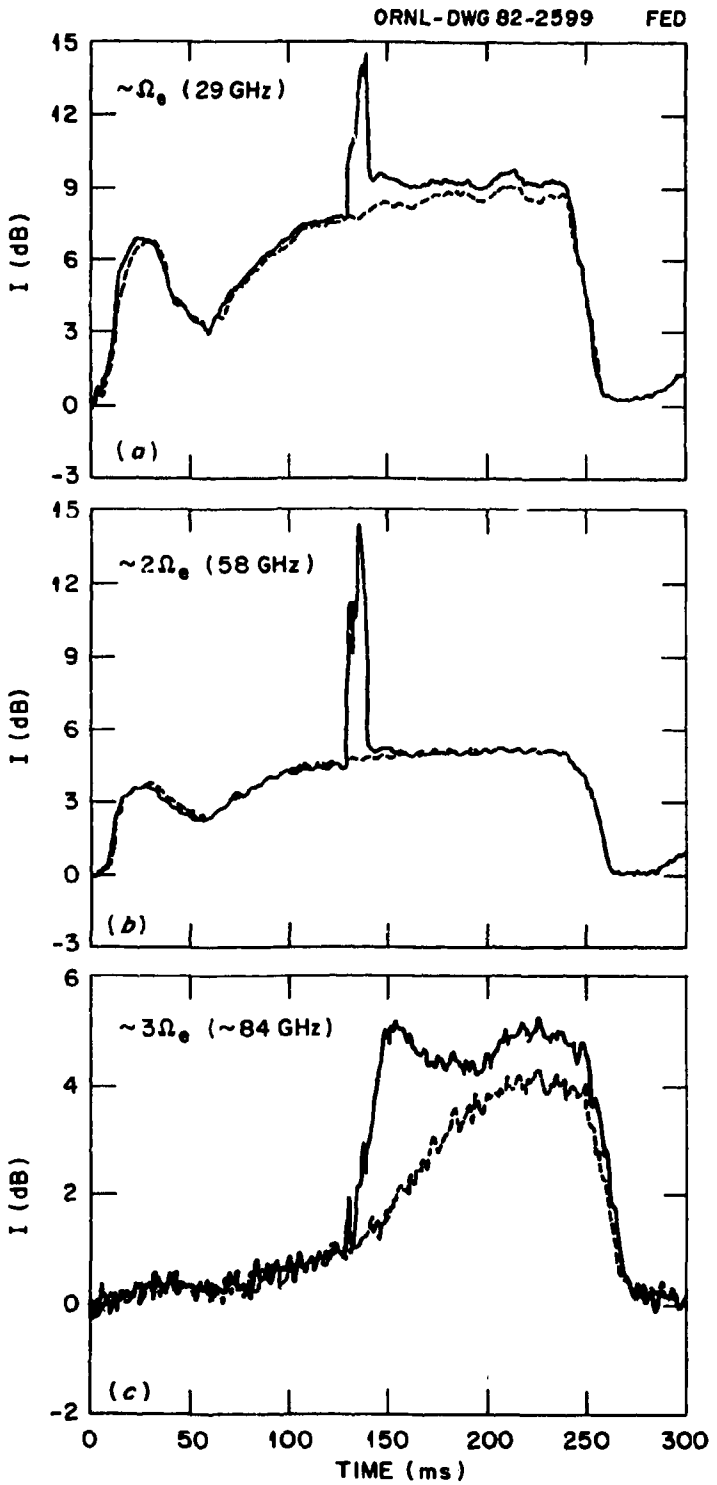

Fig. 8. ECE during a typical discharge ($n_e \sim 6.2 \times 10^{12}$ cm^{-3}) for cases with no ECH (solid line) and with an ECH pulse lasting 10 ms (dotted line). *(a)* Fundamental signal. *(b)* Second harmonic. *(c)* Third harmonic at 84.5 GHz.

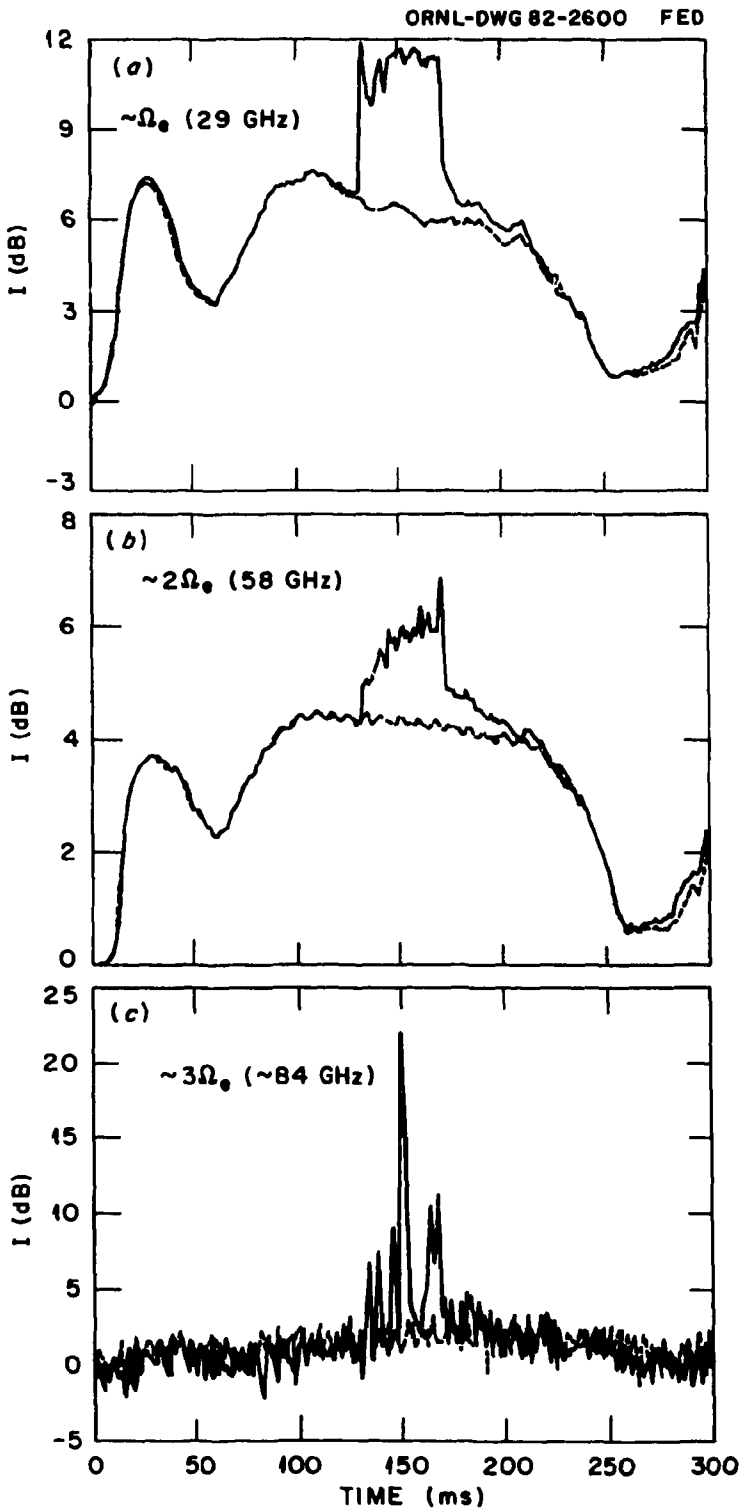

Fig. 9. ECE during a typical discharge ($n_e \sim 11.6 \times 10^{12}$ cm^{-3}) for cases with no ECH (solid line) and with an ECH pulse lasting 40 ms (dotted line). *(a)* Fundamental signal. *(b)* Second harmonic. *(c)* Third harmonic at 84.5 GHz.

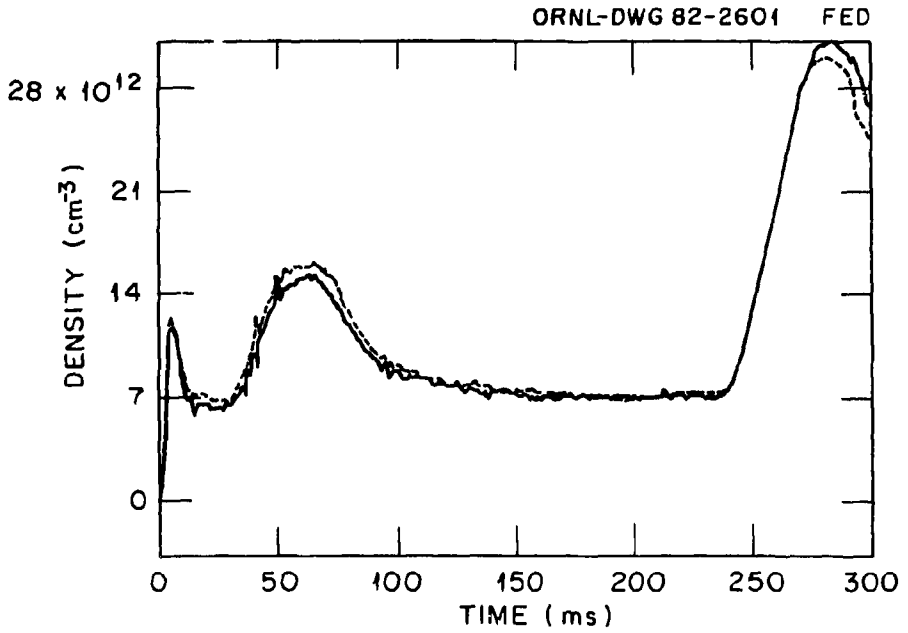

Fig. 10. The line-averaged density for typical shots with no ECH (solid line) and with ECH (dotted line). Reported values of $\langle n_e \rangle$ represent the value during the flat portion of the trace, typically taken at 130 ms.

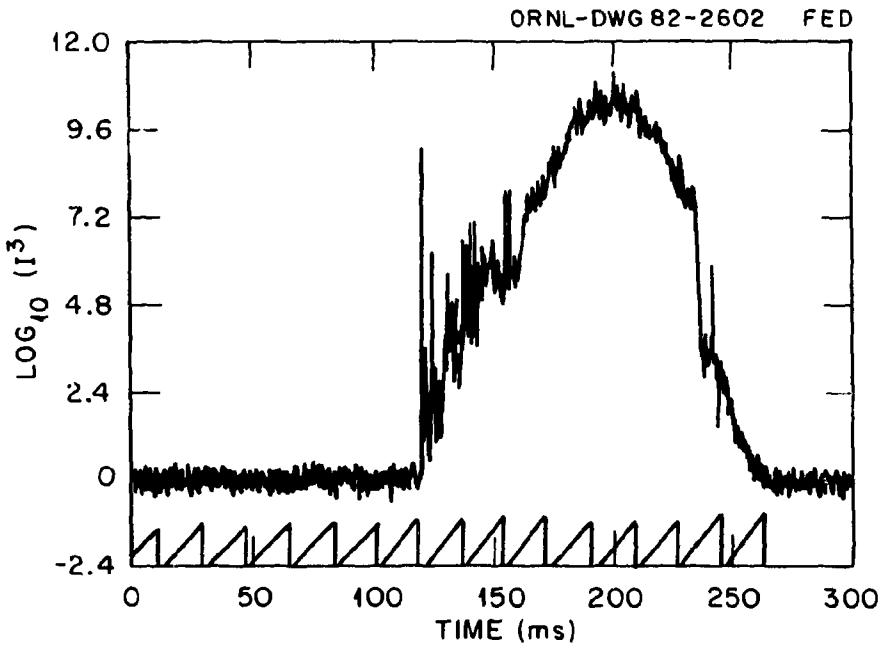

Fig. 11. The third harmonic spectrum ($n_e \sim 6.5 \times 10^{12}$ cm^{-3}); The difference between the no-ECH and ECH traces has been taken to eliminate system noise. The sawtooth at the bottom of the figure is the frequency drive, so 15 separate spectra are shown in this series. They are modulated by the overall intensity of the emissions; however, a great deal of spectral activity is apparent during the ECH pulse itself.

where the use of T_e presumes a Maxwellian distribution. Contributions from any tail electrons would be proportional to their perpendicular velocity raised to the sixth power.[14] Since the temperature and density are essentially constant during the rise of this signal, it appears that the third harmonic signal must be produced by a small tail population of energetic electrons.

A theoretical study by Gurevich[15] of the superthermal tail production in an ohmically heated plasma gives the scaling of the flux of electrons into the tail as a function of the density, temperature, and electric field. Gurevich predicts an exponential growth of the runaway flux with an algebraic decrease in density. Near the point where these two terms balance one expects that decreases in the density would lead to increasingly large changes in the runaway flux. Using values typical of ISX-B in this series of experiments, we find that a 20% decrease in the density will lead to nearly a doubling of the runaway flux. In the cases of higher-than-average density, in which there was no increase in the nonthermal emissions, a similar change of density leads to virtually no change in the runaway flux. Figure 12 shows the third harmonic signal for two cases when the line-averaged density was 2.5×10^{12} cm^{-3}. Clearly a low density is instrumental in producing a large nonthermal signature on the third harmonic emissions.

The post-ECH signal on all three harmonics in Figs. 8 and 9 is quite different from that in Fig. 7. The large rise in signal is absent and in its place is a signal that quickly approaches the no-ECH emission levels. There are two major circumstances under which this different behavior occurs. The first is illustrated in Fig. 13, where the emission characteristics have been plotted in density and plasma current ($\langle n_e \rangle$-I_p) space. If the emissions in all three systems climbed above the thermal emissions by at least 50%, the data point was plotted with a circle, while if the signals remained at their thermal levels a triangle was used. It is clear that there is a very sharp density cutoff to the enhanced emission cases, with line-averaged densities greater than approximately 6×10^{12} cm^{-3} preventing their development. A weaker dependence on the plasma current is also shown; however, within the probable error it is possible that there is no dependence on I_p.

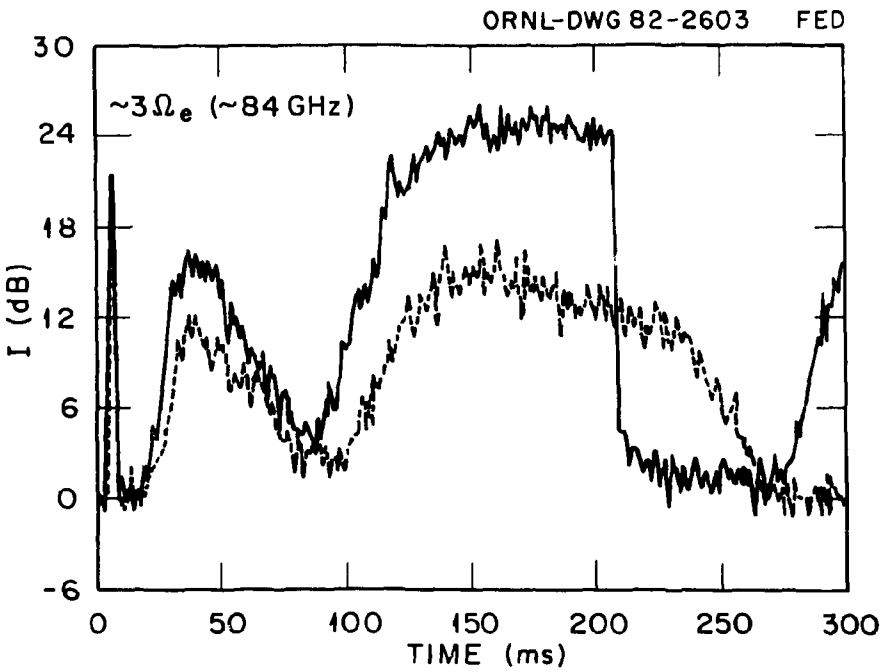

Fig. 12. The third harmonic signal in a low density discharge ($n_e \sim 10^{12}$ cm^{-3}). There is a large signal even in the case of no ECH, indicating the sensitivity of this diagnostic to the superthermal tail of the distribution.

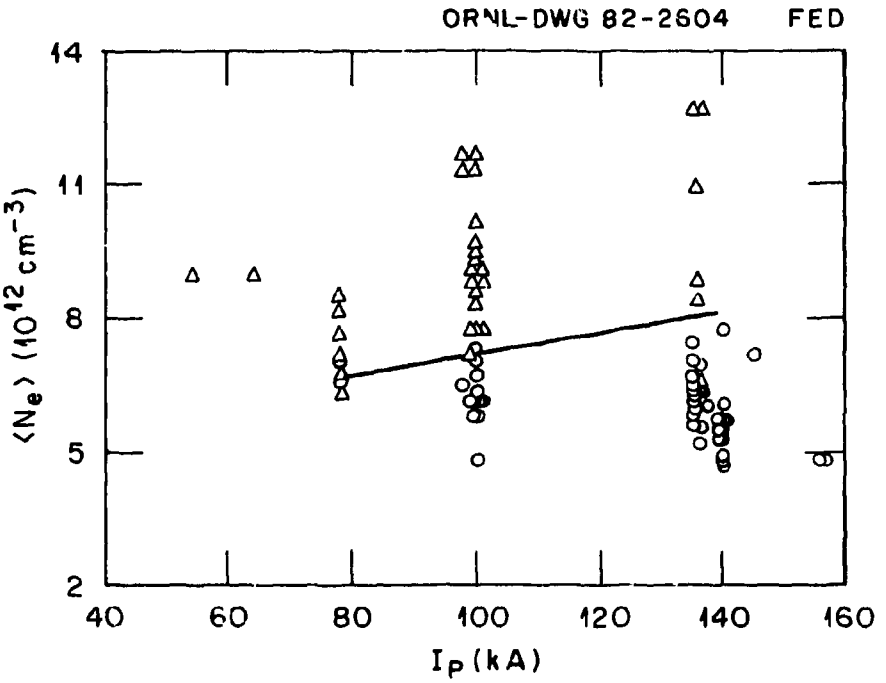

Fig. 13. Plot of density-current space for all the ECH shots. A circle was used if the third harmonic signal showed an increase after ECH of 50% or greater, while a triangle was used when the increase was less than 50%.

The second circumstance that will prevent the emergence of the large signal seen after ECH is shown in Fig. 14, where the rise of the third harmonic signal is plotted against the ECH pulse length. Most cases were quite repeatable; however, there was one case, in which the ECH was on for 20 ms and all three systems showed a major increase over their thermal levels, that could not be repeated. There is a very distinct dependence on the length of the gyrotron pulse. If the pulse length is less than 30 ms then the maximum signal is about the same as when there is no ECH; however, if the pulse length is greater than 30 ms, the signal rises to a much greater value. Also, both the lower and upper values for the increase are essentially independent of the pulse length within their respective ranges. The hatched area in Fig. 14 represents the transition region between the two cases.

The post-ECH emissions were insensitive to the location of the resonant surface in the plasma in the range between 10 cm to the outside and 10 cm to the inside. They were also independent of the occurrence of bulk electron heating. Since during this post-ECH period there was no detectable change in the loop voltage (which is altered in order to maintain the plasma current at a constant level) from the no-ECH cases, it is likely that these signals are the result of a very small population of electrons.

4.2.2 Preliminary Interpretations

In order to understand how to increase (for purposes of current drive) or decrease (to prevent the emergence of runaways during and after ECH) the tail population of electrons that appear to participate in the post-ECH effects, and in order to predict whether similar effects will be observed when higher gyrotron frequencies allow greater densities, we must come to an understanding of

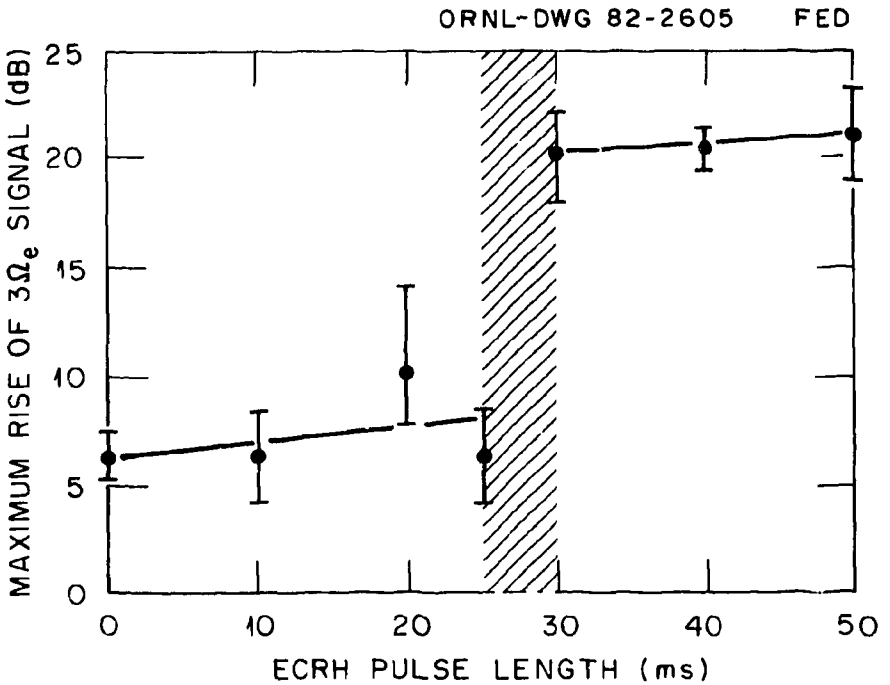

Fig. 14. The total third harmonic signal rise vs the ECH pulse length.

exactly what is being observed and what is causing the effects. This section consists of a speculative discussion of exactly these points and our preliminary conclusions. The emphasis is on the cases where there was a post-ECH rise in the emissions.

The model that this process suggests consists of four stages (shown in Fig. 15): (*a*) the pre-ECH stage, (*b*) the ECH stage, (*c*) the pitch angle scattering stage, and (*d*) the energy loss stage. In the pre-ECH stage the ohmic field pulls out a tail population of electrons. If such a tail is not pulled out, the ECH will be unable to push the electron group into a region in phase space where pitch angle scattering can operate faster than the energy damping. From the Gurevich results (Ref. 15) we see that the emergence of such a tail depends critically on a low density; therefore, Fig. 13 can be understood to represent exactly this effect. During ECH the superthermal tail is pushed up to a greater $v_\perp$ value that, in turn, increases the radiation in the harmonics. If the resulting energy of the tail particles is great enough at this stage, then the scattering processes can take place at a rate fast enough for the previous analysis to apply. If the energy is too low, then energy damping will dominate, and the emissions will not increase greatly after the gyrotron is turned off. Figure 14 may be understood to represent this fact, if the energy gained by the electrons is a function of the length of the pulse. After this occurs, the pitch angle scattering causes the emissions to increase, with the faster rate of increase being in the higher harmonics. In the experiment the fundamental signal increases more slowly than the others, as was expected. However, the second harmonic sometimes increases at a rate comparable with the third. This could be due to the interaction of the second harmonic radiated energies with the blackbody layer. Finally, energy loss or particle loss from the resonant regions results in the decay of the signal.

Estimates have been made of the scattering times required to explain the sustained 40-ms rise seen on some shots, and they show that electrons with temperatures of approximately 100 keV have the correct collision frequency. In addition, estimates made of the power emitted in the second harmonic indicate that a population of 10^5–10^8 cm^{-3} at these energies could account for the observed signal. Such a population would not show up in the plasma current, Thomson scattering, or soft x-ray data, therefore agreeing with the lack of signal on these devices.

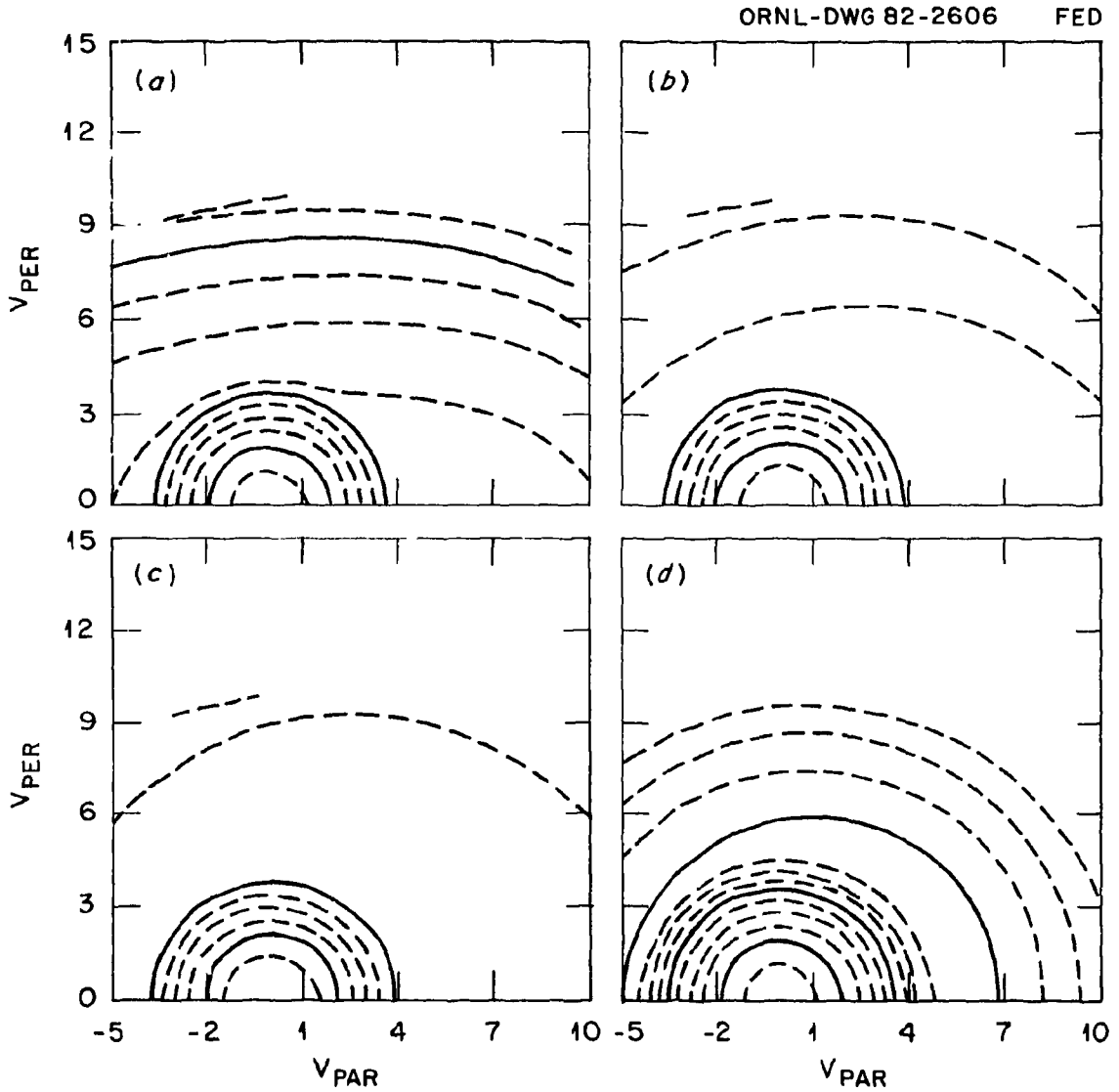

Fig. 15. Figurative representation of the proposed processes for producing the observed ECE signals. *(a)* During ohmic heating a superthermal tail of electrons is drawn out of the Maxwellian background plasma; *(b)* the ECH power raises the perpendicular energy of the tail particles; *(c)* after the ECH is turned off pitch angle scattering occurs; *(d)* the particles are lost through energy damping or by moving out of the resonance zone.

The existence of the ohmic field complicates this picture by accelerating the superthermal electrons in the $v_\parallel$ direction. This may allow lower energies for the electrons after stage (*b*). Since relativistic calculations show that the maximum energy a particle can gain from the ECH wave is limited,[16] this feature may enhance the emission. At the present time this appears to be the most likely candidate for the process causing the ECE from ISX-B.

5. CONCLUSIONS AND SUMMARY

Electron cyclotron heating of the plasma in ISX-B has been observed under low density conditions. The electron temperature rises and the loop voltage drops in reasonable agreement with it. The density also drops, as in previous experiments.

Electron cyclotron emissions at 29 GHz, 58 GHz, and 84 GHz have been observed on ISX-B during both ohmically heated and ECH discharges. The diagnostics have proven their ability to detect the existence of small changes in the electron distribution and to locate the approximate position in $v_{\parallel}$-$v_{\perp}$ space of these changes. Furthermore, an unexpected rise in the signals after the ECH pulse ends has been investigated. This rise has been attributed to the effect of pitch angle scattering on a group of electrons that were superthermal before the ECH and were then heated enough by the ECH to enable them to scatter faster than they lose their energy to the background electrons.

Currently under way at PPPL is a theoretical investigation, the goal of which is to elucidate the details of the scenario presented here. Also under consideration are other proposed explanations of the behavior of the ECE. However, none appears to be as likely to explain all of the observed data as this one.

ACKNOWLEDGMENTS

The authors gratefully acknowledge the support of M. J. Saltmarsh in making the tokamak available for these experiments and the assistance of the ISX-B operations crew under P. H. Edmonds. Diagnostic support by M. Murakami, J. L. Dunlap, V. K. Paré, D. R. Overbey, and C. E. Bush (all at ORNL), among others, was very beneficial. The aid and assistance of P. R. Brossier (Fontenay-aux-Roses) and K. Wiesen in the early phases of this work are also gratefully acknowledged, as is the support of the Princeton effort by K. Bol (PPPL). Diagnostic support by M. Goldman (PPPL) was invaluable. This work was partially supported by DOE Contract DE-ACO2-76-CHO-3073 with the Princeton Plasma Physics Laboratory.

ORNL/TM-8403
Dist. Category UC-20f

INTERNAL DISTRIBUTION

1. L. A. Berry
2–5. G. R. Dyer
6–9. O. C. Eldridge
10–13. A. C. England
14–17. J. C. Ezell
18–21. E. A. Lazarus
22–25. C. M. Loring
26. M. J. Saltmarsh
27. J. Sheffield
28–31. C. E. Thomas
32–35. J. B. Wilgen
36–37. Laboratory Records Department
38. Laboratory Records, ORNL-RC
39. Document Reference Section
40. Central Research Library
41. Fusion Energy Division Library
42. Fusion Division Reports Office
43. ORNL Patent Office

EXTERNAL DISTRIBUTION

44. Office of the Assistant Manager for Energh Research and Development, Department of Energy, Oak Ridge Operations, Box E, Oak Ridge, TN 37830
45. J. D. Callen, Department of Nuclear Engineering, University of Wisconsin, Madison, WI 53706
46. R. W. Conn, Department of Chemical, Nuclear, and Thermal Engineering, University of California, Los Angeles, CA 90024
47. S. O. Dean, Director, Fusion Energy Development, Science Applications, Inc., 2 Professional Drive, Gaithersburg, MD 20760
48. H. K. Forsen, Bechtel Group, Inc., Research Engineering, P.O. Box 3965, San Francisco, CA 94105
49. R. W. Gould, Department of Applied Physics, California Institute of Technology, Pasadena, CA 91125
50. D. G. McAlees, Exxon Nuclear Company, Inc. 777 106th Avenue, NE, Bellevue, WA 98009
51. P. J. Reardon, Princeton Plasma Physics Laboratory, P.O. Box 451, Princeton, NJ 08540
52. W. M. Stacey, Jr., School of Nuclear Engineering, Georgia Institute of Technology, Atlanta, GA 30332
53. G. A. Eliseev, I. V. Kurchatov Institute of Atomic Energy, P.O. Box 3402, 123182 Moscow, U.S.S.R.
54. V. A. Glukhikh, Scientific-Research Institute of Electro-Physical Apparatus, 188631 Leningrad, U.S.S.R.
55. I. Spighel, Lebedev Physical Institute, Leninsky Prospect 53, 117924 Moscow, U.S.S.R.
56. D. D. Ryutov, Institute of Nuclear Physics, Siberian Branch of the Academy of Sciences of the U.S.S.R., Sovetskaya St. 5, 630090 Novosibirsk, U.S.S.R.
57. V. T. Tolok, Kharkov Physical-Technical Institute, Academical St. 1, 310108 Kharkov, U.S.S.R.
58. R. Varma, Physical Research Laboratory, Navangpura, Ahmedabad, India
59. Bibliothek, Max-Planck Institut fur Plasmaphysik, D-8046 Garching bei Munchen, Federal Republic of Germany

60. Bibliothek, Institut fur Plasmaphysik, KFA, Postfach 1913, D-5170 Julich, Federal Republic of Germany
61. Bibliotheque, Centre de Recherches en Physique des Plasmas, 21 Avenue des Bains, 1007 Lausanne, Switzerland
62. Bibliotheque, Service du Confinement des Plasmas, CEA, B.P. 6, 92 Fontenay-aux-Roses (Seine), France
63. Documentation S.I.G.N., Department de la Physique du Plasma et de la Fusion Controlee, Centre d'Etudes Nucleaires, B.P. No. 85, Centre du Tri, 38041 Cedex, Grenoble, France
64. Library, Culham Laboratory, UKAEA, Abingdon, Oxon, OX14 3DB, England
65. Library, FOM Institut voor Plasma-Fysica, Rijnhuizen, Jutphaas, The Netherlands
66. Library, Institute of Physics, Academia Sinica, Beijing, Peoples Republic of China
67. Library, Institute of Plasma Physics, Nagoya University, Nagoya
68. Library, International Centre for Theoretical Physics, Trieste, Italy
69. Library, Laboratorio Gas Ionizzati, Frascati, Italy
70. Library, Plasma Physics Laboratory, Kyoto University, Gokasho Uji, Kyoto, Japan
71. Plasma Research Laboratory, Australian National University, P.O. Box 4, Canberra, A.C.T. 2000, Australia
72. Thermonuclear Library, Japan Atomic Energy Research Institute, Tokai, Naka, Ibaraki, Japan
73. A. G. Kulchar, The University of Tennessee, Knoxville, TN 37916
74. R. M. Gilgenbach, University of Michigan, Ann Arbor, MI 48109
75. H. Hsuan, Princeton Plasma Physics Laboratory, P.O. Box 451, Princeton, NJ 08540
76. G. B. Elder, Princeton Plasma Physics Laboratory, P.O. Box 451, Princeton, NJ 08540
77. K. E. Hackett, Massachusetts Institute of Technology, 77 Massachusetts Avenue, Cambridge, MA 02139
78. M. E. Read, Naval Research Laboratory, Washington, DC 20375
79. J. S. Levine, Naval Research Laboratory, Washington, DC 20375
80. K. R. Chu, Naval Research Laboratory, Washington, DC 20375
81. V. L. Granatstein, Naval Research Laboratory, Washington, DC 20375
82. F. S. McDermott, Massachusetts Institute of Technology, 77 Massachusetts Avenue, Cambridge. MA 02139
84. G. Bekefi, Massachusetts Institute of Technology, 77 Massachuusetts Avenue, Cambridge, MA 02139
85. K. Bol, Princeton Plasma Physics Laboratory, P.O. Box 451, Princeton, NJ 08540
86. J. Hosea, Princeton Plasma Physics Laboratory, P.O. Box 451, Princeton, NJ 08540
87. D. Mead, Princeton Plasma Physics Laboratory, P.O. Box 451, Princeton, NJ 08540
88. H. P. Furth, Princeton Plasma Physics Laboratory, P.O. Box 451, Princeton, NJ 08540
89. P. H. Rutherford, Princeton Plasma Physics Laboratory, P.O. Box 451, Princeton, NJ 08540
90. C. P. Moeller, GA Technologies, Inc., P.O. Box 81608, San Diego, CA 92138
91. R. Prater, GA Technologies, Inc., P.O. Box 81608, San Diego, CA 92138
92. V. V. Alikaev, Kurchatov Institute of Atomic Energy, P.O. Box 3402, 123182 Moscow, U.S.S.R.
93. K. A. Razumova,, Kurchatov Institute of Atomic Energy, P.O. Box 3402, 123182 Moscow, U.S.S.R.
94. D. G. Buliginski, A. F. Iofffe Physico-Technical Institute, 194021 Leningrad, U.S.S.R.
95. V. E. Golant, A. F. Iofffe Physico-Technical Institute, 194021 Leningrad, U.S.S.R.
96. M. M. Larionov, A. F. Iofffe Physico-Technical Institute, 194021 Leningrad, U.S.S.R.
97. K. N. Stepanov, Kharkov Physical-Technical Institute, Academical St. 1, 310108 Kharkov, U.S.S.R.

98. V. T. Tolok, Kharkov Physical-Technical Institute, Academical St. 1, 310108 Kharkov, U.S.S.R.

99–278. Given distribution as shown in TID-4500 Magnetic Fusion Energy (Category Distribution UC-20f)

19/20

REFERENCES

1. R. M. Gilgenbach et al., *Phys. Rev. Lett.* **44,** 647 (1980).
2. R. M. Gilgenbach et al., *Nucl. Fusion* **21,** 319 (1981).
3. R. D. Wengenroth, *IEEE Trans. Microwave Theory Techn.* **MTT-26,** 332 (1978).
4. G. Campen et al., *Proc. 8th Symp. on Engineering Problems of Fusion Research* (IEEE, 1979), Vol. II, p. 960.
5. A. G. Kulchar et al., *Second Cyclotron Harmonic Emission Measurements on ISX-B,* ORNL/TM-8200, Oak Ridge National Laboratory, Oak Ridge, Tennessee (1982).
6. I. Fidone et al., *Phys. Fluids* **23,** 1336 (1980); TFR Group and I. Fidone, *Phys. Rev. A* **24,** 2861 (1981).
7. G. Elder and H. Hsuan, *Bull. Am. Phys. Soc.* **25,** 1004 (1980).
8. C. P. Moeller, *Proc. 4th Topical Conf. on Radio Frequency* (University of Texas, Austin, 1981), paper D1; C. P. Moeller et al., *Phys. Fluids* **25,** 1211 (1982); and C. P. Moeller et al., *Electron Cyclotron Heating Experiment on the JFT-2 Tokamak Using an Inside Launch Antenna,* GA-A16397, General Atomic Co., San Diego, Calif. (1981).
9. V. V. Alikaev et al., *Sov. Phys.-JETP* **35,** 115 (1982).
10. I. Fidone, G. Granata, and R. L. Meyer, EUR-CEA-FC-1136, Centre d'Etudes Nucléaires, Fontenay-aux-Roses, France (December 1981).
11. V. Arunasalam, P. Efthimion, and J. Hosea, *Bull. Am. Phys. Soc.* **26,** 907 (1981).
12. S. McDermott, G. Bekefi, K. E. Hackett, J. S. Levine, and M. Porkolab, *Phys. Fluids* **25,** 1488 (1982).
13. C. Celata and D. Boyd, *Nucl. Fusion* **13,** 497 (1973).
14. G. Bekefi, *Radiation Processes in Plasma,* John Wiley and Sons, Inc., New York, 1966.
15. A. V. Gurevich, Ya. S. Dimant, Yu. N. Dnestrovskii, and A. P. Smirnov, *Sov. J. Plasma Phys.* **5,** 437 (1979).
16. G. Elder, *Bull. Am. Phys. Soc.* **25,** 1004 (1980).